SCIENCE CHINA
Physics, Mechanics & Astronomy

• Article •

October 2021 Vol. 64 No. 10: 108712
https://doi.org/10.1007/s11433-021-1752-0

Cis-interaction of ligands on a supported lipid bilayer affects their binding to cell adhesion receptors

Long Li[1], Jinglei Hu[2,3*], Huaping Wu[4*], and Fan Song[1,5*]

[1] *State Key Laboratory of Nonlinear Mechanics (LNM) and Beijing Key Laboratory of Engineered Construction and Mechanobiology, Institute of Mechanics, Chinese Academy of Sciences, Beijing 100190, China;*
[2] *Kuang Yaming Honors School & Institute for Brain Sciences, Nanjing University, Nanjing 210023, China;*
[3] *Shenzhen Research Institute, Nanjing University, Shenzhen 518057, China;*
[4] *College of Mechanical Engineering, Zhejiang University of Technology, Hangzhou 310023, China;*
[5] *School of Engineering Science, University of Chinese Academy of Sciences, Beijing 100049, China*

Received May 11, 2021; accepted July 23, 2021; published online September 3, 2021

Cell adhesion on a supported lipid bilayer (SLB) functionalized with ligand proteins is a widely-used cell-mimetic model for the study of the *trans* receptor-ligand interaction that mediates the adhesion, and has been shown to play an important role in unravelling the molecular players in cell adhesion. Experimental studies of such cell-SLB adhesion systems often assume that there is no *cis* interactions between the ligands. An important question remains whether the *cis*-interaction affects the *trans* receptor-ligand interaction. Using a statistical-mechanical model and Monte Carlo simulations with biologically relevant parameters, we find that the attractive *cis*-interaction of strength $1\,k_BT$ between adjacent ligands on the SLB can lead to an amplification of both the affinity and cooperativity of the receptor-ligand binding, thereby facilitating the phase separation within the adhering cell membrane. In contrast, the adhesion system is less sensitive to the repulsive *cis*-interaction between adjacent ligands on the SLB. Our results suggest that the ligand-ligand *cis*-interaction should be carefully considered in the cell-SLB adhesion experiments.

cell adhesion, ligand-ligand *cis*-interaction, receptor-ligand interaction, phase behavior

PACS number(s): 87.15.A-, 87.15.K-, 87.16.D-, 87.17.Rt

Citation: L. Li, J. Hu, H. Wu, and F. Song, *Cis*-interaction of ligands on a supported lipid bilayer affects their binding to cell adhesion receptors, Sci. China-Phys. Mech. Astron. **64**, 108712 (2021), https://doi.org/10.1007/s11433-021-1752-0

1 Introduction

Cell adhesion is essential for tissue formation, immune response, cell signaling and locomotion. The adhesion process is caused by the binding of cell surface receptors to their cognate ligands presented on the neighboring cell, and is implicated by intracellular adaptor proteins and cytoskeletal filaments [1-4]. To identify the receptor-ligand pairs and elucidate physical interactions at the membrane interface, supported lipid bilayers (SLB's) decorated with protein ligands have been widely used as reconstituted model systems or artificial target cells [5-7]. For example, SLB's containing antigenic peptide-major histocompatibility complex (pMHC) molecules were used as a minimal model of antigen presenting cells to demonstrate that pMHC complexes are the ligand for T-cell receptors [5]. Dustin et al. [8] confirmed that

*Corresponding authors (Jinglei Hu, email: hujinglei@nju.edu.cn; Huaping Wu, email: wuhuaping@gmail.com; Fan Song, email: songf@lnm.imech.ac.cn)

lymphocyte function-associated antigen 3 (LFA-3) is a ligand for CD2 from adhesion experiments of $CD2^+$ T lymphocytes with SLB's bearing purified LFA-3. Biswas et al. [9] showed that the initial stage of epithelial (E)-cadherin junction formation depends on the *trans* but not the *cis* interactions between E-cadherins from cell-SLB adhesion experiments. Schmid et al. [10] studied the size-dependent exclusion of non-binding proteins from the adhesion zone formed between giant unilamellar vesicles and SLB's via the binding of synthetic proteins.

Among the important physical interactions at the membrane interface is the receptor-ligand binding interaction, which is quantified by the apparent equilibrium constant $K = [\mathrm{RL}]/([\mathrm{R}][\mathrm{L}])$ [11-14] with [RL], [R] and [L] the area concentrations of receptor-ligand complexes, free receptors and free ligands, respectively. A variety of experimental techniques have been attempted to measure K [15-19]. Theoretical modeling [20], computer simulations [21-25] and very recent experiment [26] have shown that K depends not only on the interaction of the binding proteins, but also on such membrane properties as thermal roughness, membrane microdomains exhibiting affinity for the proteins, and bending rigidity. These studies provide insights into our understanding of the receptor-ligand binding in the two-dimensional membrane environment and often assume that there was no direct *cis* interaction between the receptors or ligands. In fact, the receptors or ligands may experience *cis* interactions due to electrostatics. For example, cadherins are known to attract each other on the same membrane [1, 13]. It remains to be understood how the *cis* interaction affects the receptor-ligand binding, especially in the cell-SLB adhesion.

Here we report the study of a cell membrane adhering to a SLB as shown in Figure 1. The adhesion receptors are weakly coupled to the nanoclusters enriched in saturated lipids and cholesterol within the cell membrane. Such coupling was reported in biological experiments [27-29]. The mobile ligands on the SLB experience short-range *cis* attraction or repulsion. From mean-field (MF) calculations and Monte Carlo (MC) simulations, we find that, in the biologically relevant range of model parameters, an attraction of one k_BT between adjacent ligands on the SLB can significantly alter the receptor-ligand binding and therefore the behavior of the adhesion system. Our results suggest that the ligand-ligand *cis*-interaction should be carefully considered in the cell-SLB adhesion experiments.

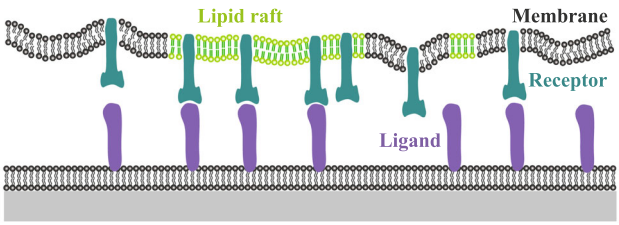

Figure 1 (Color online) Cartoon of the contact zone of a cell membrane adhering to a supported lipid bilayer via the receptor-ligand binding. The cell adhesion receptors (dark green) exhibit weak affinity for the lipid rafts (light green) within the cell membrane. The ligands (purple) may experience short-range attraction or repulsion.

2 Model and methods

Cell adhesion involves length scales that differ by orders of magnitude, ranging from angstroms (specific receptor-ligand binding), to tens of nanometers (receptor-ligand complex), and to micrometers (lateral size of a typical cell adhesion zone). To deal with the multiscale problem involved in the biological system, we employ a statistical-mechanical model that has been widely used to study both the equilibrium [14, 30] and dynamic adhesion behaviors [31, 32]. The configurational energy of the adhesion system contains contributions from the membrane bending energy $\mathcal{H}_{\mathrm{me}}$, the receptor-ligand binding interaction $\mathcal{H}_{\mathrm{R\text{-}L}}$, the ligand-ligand *cis*-interaction $\mathcal{H}_{\mathrm{L\text{-}L}}$, the contact energy of neighboring lipid-raft patches within the cell membrane $\mathcal{H}_{\mathrm{r\text{-}r}}$, as well as the coupling energy between lipid rafts and adhesion receptors $\mathcal{H}_{\mathrm{r\text{-}R}}$.

In our model, the cell membrane and SLB are described as discretized elastic surfaces with quadratic patches of size a^2, as shown in Figure 2. Stimulated by Brownian motion of water molecules, the cell membrane undergoes transverse fluctuations in shape. In contrast, the thermal shape fluctuation of SLB is totally suppressed due to the presence of supported planar substrate. The conformation of the cell membrane can be described in Monge representation via the height field with respect to a reference horizontal plane. The bending energy of the cell membrane is then given by [25, 33]

$$\mathcal{H}_{\mathrm{me}} = \frac{\kappa}{2a^2}\sum_i (\Delta_{\mathrm{d}} l_i)^2 , \tag{1}$$

where κ is the bending rigidity of the cell membrane, and $\Delta_{\mathrm{d}} l_i$ is the discretized Laplacian of the height field $\{l_i\}$ between cell membrane and SLB at lattice site i.

We set the length unit of the model $a = 10$ nm to match the exclusion radius of membrane proteins [34]. Each lattice of size a^2 can accommodate one single receptor or ligand molecule, in analogy to the lattice gas model. The spatial distribution of receptors in the upper cell membrane is described by the composition field $\{m_i^+\}$ with values $m_i^+ = 0$ or 1 indicating the absence or presence of receptor at patch i. Likewise, $\{m_i^-\}$ with values $m_i^- = 0$ or 1 describes the spatial distribution of ligands in the lower SLB. One receptor only

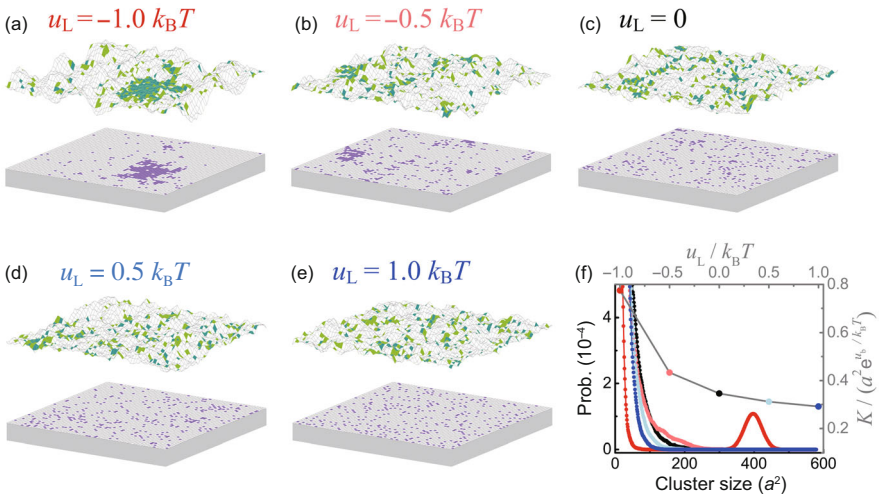

Figure 2 (Color online) Results from MC simulations of the adhesion systems with short-range interaction of strength u_L between adjacent ligands. (a)-(e) Simulation snapshots at different values of u_L as specified. $u_L < 0$ means attraction, and $u_L > 0$ repulsion. Lipid rafts, receptors, and ligands are modeled by single square patches of size a^2 with the same color coding as in Figure 1. (f) Distribution of the lipid-raft cluster size and the receptor-ligand binding constant K as a function of u_L for the corresponding systems shown in (a)-(e). The other parameters for these adhesion systems are the same, i.e., the area fraction of rafts within the cell membrane $x = 0.2$, area concentration of receptors and ligands $c_R = c_L = 1000\,\mu m^{-2}$, receptor-ligand binding strength $u_b = 6\,k_BT$, raft-receptor affinity $u_a = 3\,k_BT$, and raft-raft contact energy $u = 0.8\,u^*$ with the critical value $u^* = -2\ln\left(1+\sqrt{2}\right) k_BT$ according to the exact solution of the lattice gas model on a square lattice.

binds one ligand if they are located at opposite membrane patches and their distance l_i is within the binding range, i.e., $l_c - l_b/2 < l_i < l_c + l_b/2$, where l_c is the length of receptor-ligand complex and l_b the width of the square-well binding potential V_b. The interaction energy of receptors and ligands within the contact zone is described by [35,36]

$$\mathcal{H}_{\text{R-L}} = \sum_i V_b m_i^+ m_i^- = -u_b \sum_i m_i^+ m_i^- \theta\left(\frac{l_b}{2} - |l_i - l_c|\right), \quad (2)$$

where $u_b > 0$ is the binding energy, $\theta(\cdots)$ is the Heaviside's step function, implying that a complex cannot be formed if the two adhesion proteins are separated beyond the binding range. The potential in eq. (2) incorporates the distance- and orientation-dependence of the binding interaction and therefore effectively takes into account the binding specificity of the adhesion proteins. For flexible adhesion proteins, their conformation might play a role in the binding, which is not included in our work and requires molecular modeling via detailed models, e.g., the bead-spring model for polymer chains. The conformational flexibility of adhesion proteins shall be addressed in future studies.

In addition to the *trans* receptor-ligand binding, we also consider the *cis*-interaction between ligands on the SLB. Specifically, any two nearest-neighboring ligands interact with an energy of u_L. $u_L > 0$ accounts for repulsion and $u_L < 0$ attraction. The total ligand-ligand interacting energy is then

$$\mathcal{H}_{\text{L-L}} = u_L \sum_{\langle i,j \rangle} \left(m_i^- m_j^-\right), \quad (3)$$

which essentially sums over all pairs of nearest-neighbor patches $\langle i, j \rangle$ occupied by ligands on the SLB.

The lipid rafts in the cell membrane are represented by dynamic clusters of square patches. The spatial distribution of raft patches is described by the composition fields $\{n_i^+\}$ with values 0 or 1 indicating, respectively, the absence or presence of lipid rafts in cell membrane at lattice site i. Since lipid rafts *in vivo* are highly dynamic microdomains which undergo merging and fission, we introduce a contact energy u between the nearest-neighbor raft patches. The total raft-raft contact energy can be written as [24]:

$$\mathcal{H}_{\text{r-r}} = u \sum_{\langle i,j \rangle} \left(n_i^+ n_j^+\right). \quad (4)$$

The lipid rafts tend to coalesce and form larger domains for a contact energy $u < 0$.

To take into account the fact that protein molecules prefer raft domains of the membranes, we introduce the energy decrease u_a for a receptor to partition into a raft domain from the non-raft region of the membrane, i.e., the raft affinity to receptors. The total raft-receptor association energy is then written as [37]:

$$\mathcal{H}_{\text{r-R}} = -u_a \sum_i \left(n_i^+ m_i^+\right). \quad (5)$$

The overall configurational energy $\mathcal{H}_{\text{ad}} = \mathcal{H}_{\text{me}} + \mathcal{H}_{\text{R-L}} + \mathcal{H}_{\text{L-L}} + \mathcal{H}_{\text{r-r}} + \mathcal{H}_{\text{r-R}}$ defines the adhesion system studied here.

2.1 Monte Carlo simulations

We use the MC simulation method with the standard Metropolis algorithm to study the adhesion system. The simulation process involves three types of MC trial moves: (1) transverse displacements of upper membrane patches to capture thermally-excited shape fluctuations of the cell membrane, (2) lateral translations of proteins and (3) lateral translations of raft patches to mimic their diffusion. To prevent the overlap of the two surfaces, all trial moves of type (1) leading to $l_i < 0$ are rejected. By omitting the trial move of type (1), we also perform MC simulations for the control adhesion systems with planar membranes at a fixed separation $l_i = l_c$ relative to the SLB in order to appreciate the role of membrane shape fluctuations. The diffusive motion of proteins and rafts is modeled as a hopping process. Each receptor, ligand or lipid raft can hop to one of the four nearest-neighbor lattices with equal probability. The lipid rafts in the cell membrane move independently of the receptor molecules. The trial moves of type (1) leads to possible variations in $\mathcal{H}_{\rm me}$ and $\mathcal{H}_{\rm R\text{-}L}$, type (2) in $\mathcal{H}_{\rm R\text{-}L}$, $\mathcal{H}_{\rm L\text{-}L}$ and $\mathcal{H}_{\rm r\text{-}R}$, and type (3) in $\mathcal{H}_{\rm r\text{-}r}$ and $\mathcal{H}_{\rm r\text{-}R}$. The proportion of these trial moves in each MC sweep (MCS) is chosen according to the physical timescales as in our earlier work [24]. The trial moves will be accepted or rejected according to the standard Metropolis algorithm. One MC sweep corresponds roughly to a physical time of 10 μs, since the time for the proteins traveling a distance of $a = 10$ nm to a neighboring lattice site is of the order of 10 μs as estimated by $t = a^2/4D$ with the typical diffusion coefficient $D = 1\ \mu\text{m}^2/\text{s}$ [38, 39] for membrane proteins. To identify phase transitions in the adhesion system, we use the method adopted in the Ising model to measure the $C_{\rm V} = (\langle\mathcal{H}_{\rm ad}^2\rangle - \langle\mathcal{H}_{\rm ad}\rangle e^2)/(Nk_{\rm B}T^2)$ as a function of system variable, i.e., raft-raft contact energy u (see Figure a1 in Appendix). Here, N is the total number of lattice sites and the angular brackets $\langle\ldots\rangle$ denote the ensemble average. We calculate the receptor-ligand binding constant K = [RL]/([R][L]) by computing the area concentration [RL] of the receptor-ligand complexes, [R] of free receptors and [L] of free ligands in the simulations.

We have performed simulations with the membrane area of $A_{\rm me} = 600\ \text{nm} \times 600\ \text{nm}$ under periodic boundary conditions. In each of the MC simulations, a relaxation run of 5×10^7 MCS is performed for thermal equilibration and a subsequent run of 5×10^7 MCS for statistical sampling. The simulation parameters are chosen according to existing literature data. Specifically, the bending rigidity of the lipid membrane has a typical value of $\kappa = 10\ k_{\rm B}T$ [22] with $k_{\rm B}$ and T being the Boltzmann constant and physiological temperature, respectively. To define the square-well potential, we choose binding energy $u_{\rm b} = 3\ k_{\rm B}T$ to $6\ k_{\rm B}T$, potential range $l_{\rm b}$ = 1 nm, and complex length $l_{\rm c} = 15$ nm [20, 36]. To obtain the experimentally measured protein concentration in the lipid rafts, which is in the range of around 10^3 to 10^4 molecules per μm^2 [40], the raft affinity to receptor molecules $u_{\rm a} = 2\ k_{\rm B}T$ to $4\ k_{\rm B}T$ is adopted. We vary the area concentration of ligand up to $0.1a^{-2}$, which corresponds to a maximal concentration of 1000 μm^{-2} [21]. In our simulations the area fraction of the raft domains $x = 0.2$ unless otherwise specified [24, 41]. The adhesion proteins and lipid rafts are all randomly distributed in the apposing surfaces at the beginning of each simulation. Note that these initial distributions of proteins and lipid rafts, however, do not affect the binding constant and phase behavior, since the equilibrium quantities do not depend on the dynamic properties of the systems.

2.2 Mean field theory

We also perform calculations of the adhesion system based on the MF theory. We start with the grand-canonical ensemble in which the concentrations of adhesion proteins and lipid rafts are adjusted by the chemical potentials $\mu_{\rm p}$ and $\mu_{\rm r}$. The configurational energy of the system in the grand-canonical ensemble is

$$\mathcal{H} = \mathcal{H}_{\rm ad} - \mu_{\rm r}\sum_i n_i^+ - \sum_i \left(\mu_{\rm R} m_i^+ + \mu_{\rm L} m_i^-\right). \tag{6}$$

Transforming raft and protein variables $n_i^+ = 0, 1$ and $m_i^- = 0, 1$ to spin variables $s_i^+ = 2n_i^+ - 1 = \pm 1$ and $t_i^- = 2m_i^- - 1 = \pm 1$, and using MF approximation $s_i^+ s_j^+ \approx \langle s_i^+\rangle s_i^+ + \langle s_j^+\rangle s_j^+ - \langle s_i^+\rangle\langle s_j^+\rangle$ with the average $s = \langle s_i^+\rangle = \langle s_j^+\rangle$, $t_i^- t_j^- \approx \langle t_i^-\rangle t_i^- + \langle t_j^-\rangle t_j^- - \langle t_i^-\rangle\langle t_j^-\rangle$ with the average $t = \langle t_i^-\rangle = \langle t_j^-\rangle$, we obtain MF Hamiltonian

$$\begin{aligned}\mathcal{H}_{\rm MF} =& \mathcal{H}_{\rm me} + \mathcal{H}_{\rm R\text{-}L} + \sum_i \left[\epsilon_{\rm r}^+ + \epsilon_{\rm p}^- - U_{\rm effr} s_i^+ - U_{\rm effL} t_i^-\right] \\ &+ \sum_i \left[\frac{u_{\rm a}}{2}(s_i^+ + 1)\, m_i^+ + \frac{V_{\rm b}}{2}(t_i^- + 1)\, m_i^+ - \mu_{\rm R} m_i^+\right],\end{aligned} \tag{7}$$

with $\epsilon_{\rm r}^+ = \frac{1}{2}\left[-u(s^2-1) - \mu_{\rm r}^+\right]$, $\epsilon_{\rm L} = \frac{1}{2}\left[-u_{\rm L}(t^2-1) - \mu_{\rm p}^-\right]$, $U_{\rm effr} = -u(1+s) + \frac{1}{2}\mu_{\rm r}^+$, $U_{\rm effL} = -u_{\rm L}(1+t) + \frac{1}{2}\mu_{\rm L}$. Then the grand-canonical partition function is given by

$$\begin{aligned}\mathcal{Z}_{\rm MF} =& \left[\prod_i \int_0^\infty {\rm d}l_i\right]\left[\prod_i \sum_{s_i^+=\pm1}\sum_{t_i^-=\pm1}\sum_{m_i^+=0,1}\right] {\rm e}^{-\beta\mathcal{H}_{\rm MF}} \\ =& {\rm e}^{-N\beta(\epsilon_{\rm r}^+ + \epsilon_{\rm p}^-)}\left[\prod_i \int_0^\infty {\rm d}l_i\right] \\ &\times\left[{\rm e}^{-\beta\mathcal{H}_{\rm me}}\prod_i \sum_{\sigma^+=\pm1}\sum_{\sigma^-=\pm1} w_{\sigma^+,\sigma^-}(l_i)\right],\end{aligned} \tag{8}$$

with $\beta = (k_{\rm B}T)^{-1}$ and

$$w_{\sigma^+,\sigma^-}(l_i) = \left[{\rm e}^{\beta\left(U_{\rm effr}\sigma^+ + U_{\rm effL}\sigma^-\right)} + {\rm e}^{\beta\left(U_{\rm effr}\sigma^+ + U_{\rm effL}\sigma^-\right)}\right.$$

$$\times \mathrm{e}^{\beta\left(-\frac{1}{2}u_{\mathrm{a}}(\sigma^{+}+1)-\frac{1}{2}u_{\mathrm{b}}\theta(l_{\mathrm{b}}/2-|l_i-l_{\mathrm{c}}|)(\sigma^{-}+1)+\mu_{\mathrm{R}}\right)}\Big]. \tag{9}$$

By defining $A_{\sigma^+,\sigma^-} = w_{\sigma^+,\sigma^-}(l_i)|_{\theta(l_{\mathrm{b}}/2-|l_i-l_{\mathrm{c}}|)=0}$ and $B_{\sigma^+,\sigma^-} = w_{\sigma^+,\sigma^-}(l_i)|_{\theta(l_{\mathrm{b}}/2-|l_i-l_{\mathrm{c}}|)=1}$, the partition function given by eq. (8) can be rewritten as:

$$\mathcal{Z}_{\mathrm{MF}} = \mathrm{e}^{-N\beta(\epsilon_{\mathrm{r}}^{+}+\epsilon_{\mathrm{p}}^{-})}\left[\sum_{\sigma^+=\pm1}\sum_{\sigma^-=\pm1}A_{\sigma^+,\sigma^-}\right]^{N} \times\left[\prod_i\int_0^{\infty}\mathrm{d}l_i\right]\mathrm{e}^{-\beta\left[\mathcal{H}_{\mathrm{me}}+\sum_i V_{\mathrm{b,eff}}(l_i)\right]}, \tag{10}$$

where the effective binding potential $V_{\mathrm{b,eff}}(l_i) = -U_{\mathrm{b,eff}}\theta(l_{\mathrm{b}}/2-|l_i-l_{\mathrm{c}}|)$ is a square-well potential of the same width l_{b} and location l_{c} as the receptor-ligand binding potential in eq. (2). The effective binding strength

$$U_{\mathrm{b,eff}} = k_{\mathrm{B}}T\ln\frac{\sum_{\sigma^+}\sum_{\sigma^-}B_{\sigma^+,\sigma^-}}{\sum_{\sigma^+}\sum_{\sigma^-}A_{\sigma^+,\sigma^-}} \tag{11}$$

is a function of parameters u_{b}, u_{a}, u, μ_{p}, μ_{r} and T. The free energy per lattice site is

$$\mathcal{F} = -\frac{k_{\mathrm{B}}T}{N}\ln\mathcal{Z}_{\mathrm{MF}} = \epsilon_{\mathrm{r}}^{+}+\epsilon_{\mathrm{p}}^{-}-k_{\mathrm{B}}T\ln\left[\sum_{\sigma^+=\pm1}\sum_{\sigma^-=\pm1}A_{\sigma^+,\sigma^-}\right]+\mathcal{F}_0, \tag{12}$$

where

$$\mathcal{F}_0 = -\frac{k_{\mathrm{B}}T}{N}\ln\left\{\left[\prod_i\int_0^{\infty}\mathrm{d}l_i\right]\mathrm{e}^{-\beta\left[\mathcal{H}_{\mathrm{me}}+\sum_i V_{\mathrm{b,eff}}(l_i)\right]}\right\} \tag{13}$$

is the free energy per lattice site for the reference system of two homogeneous membranes with Hamiltonian $\mathcal{H}_0 = \mathcal{H}_{\mathrm{me}} + \sum_i V_{\mathrm{b,eff}}(l_i)$.

Phase separation occurs if $\mathcal{F}$ exhibits two equal minima separated by a maximum, implying that $\partial\mathcal{F}/\partial s = \partial\mathcal{F}/\partial t = 0$ has three roots, and $\partial^2\mathcal{F}/\partial s^2$ and $\partial^2\mathcal{F}/\partial t^2$ are negative for one of the roots and positive for the other two. The condition $\partial\mathcal{F}/\partial s = 0$ leads to the self-consistent equation

$$s = P_{\mathrm{b}}\frac{\sum_{\sigma^+}\sum_{\sigma^-}\sigma^{+}B_{\sigma^+,\sigma^-}}{\sum_{\sigma^+}\sum_{\sigma^-}B_{\sigma^+,\sigma^-}} + (1-P_{\mathrm{b}})\frac{\sum_{\sigma^+}\sum_{\sigma^-}\sigma^{+}A_{\sigma^+,\sigma^-}}{\sum_{\sigma^+}\sum_{\sigma^-}A_{\sigma^+,\sigma^-}}, \tag{14}$$

where $P_{\mathrm{b}} = -\partial\mathcal{F}_0/\partial U_{\mathrm{b,eff}} = \langle\theta(l_{\mathrm{b}}/2-|l_i-l_{\mathrm{c}}|)\rangle$ is the so-called contact probability of the homogeneous membranes in the aforementioned reference system. Specifically, $0 \le P_{\mathrm{b}} \le 1$ is the expectation value for the fraction of bound membrane patches, i.e., membrane patches with $l_{\mathrm{c}} - l_{\mathrm{b}}/2 < l_i < l_{\mathrm{c}} + l_{\mathrm{b}}/2$ in the reference system. Similarly, the condition $\partial\mathcal{F}/\partial t = 0$ leads to the self-consistent equation

$$t = P_{\mathrm{b}}\frac{\sum_{\sigma^+}\sum_{\sigma^-}\sigma^{-}B_{\sigma^+,\sigma^-}}{\sum_{\sigma^+}\sum_{\sigma^-}B_{\sigma^+,\sigma^-}} + (1-P_{\mathrm{b}})\frac{\sum_{\sigma^+}\sum_{\sigma^-}\sigma^{-}A_{\sigma^+,\sigma^-}}{\sum_{\sigma^+}\sum_{\sigma^-}A_{\sigma^+,\sigma^-}}. \tag{15}$$

In the case of fluctuating membranes we determine P_{b} by simulating the reference system of two homogeneous membranes with Hamiltonian $\mathcal{H}_0$. In the case of two planar membranes within the receptor-ligand binding range, i.e., with $\theta(l_{\mathrm{b}}/2 - |l_i - l_{\mathrm{c}}|) = 1$ at any site i, $P_{\mathrm{b}} = 1$. We then identify the phase transition points by numerically solving eqs. (14) and (15) under the same constraint as for the adhesion system that the solutions shall lead to equal minima of the free energy $\mathcal{F}$.

3 Results and discussion

The MC simulation snapshots in Figure 2(a)-(e) clearly illustrate that the short-range interaction of strength u_{L} between adjacent ligands (purple) on the supported lipid bilayers impacts the spatial organization of receptors (dark green) and lipid rafts (light green) within the adhering cell membranes. In these adhesion systems all the other parameters except u_{L} are kept the same, i.e., area fraction of rafts within the cell membranes $x = 0.2$, area concentration of receptors and ligands $c_{\mathrm{R}} = c_{\mathrm{L}} = 1000\,\mu\mathrm{m}^{-2}$, receptor-ligand binding strength $u_{\mathrm{b}} = 6\,k_{\mathrm{B}}T$, raft-receptor affinity $u_{\mathrm{a}} = 3\,k_{\mathrm{B}}T$, and raft-raft contact energy $u = 0.8\,u^*$ with the critical value $u^* = -2\ln\left(1+\sqrt{2}\right)k_{\mathrm{B}}T$ according to the exact solution of the lattice gas model on a square lattice. Here, u^* also corresponds to the critical contact energy required for the transition from the homogeneous to phase-separated state for a planar membrane containing lipid rafts. Comparison of the snapshots reveals that, ligand-ligand attraction ($u_{\mathrm{L}} < 0$) leads to the domain formation on both surfaces, whereas ligand-ligand repulsion ($u_{\mathrm{L}} > 0$) tends to disperse the adhesion receptors and lipid rafts. Although the ligand-ligand interaction has a short range of $a = 10$ nm less than the average spacing $\bar{d} = c_{\mathrm{L}}^{-1/2} = 31.6$ nm between ligands, a strength of $u_{\mathrm{L}} = \pm1.0\,k_{\mathrm{B}}T$ for this interaction can significantly alter the behavior of the adhesion systems. The distribution of lipid-raft cluster size in Figure 2(f) shows that, the single peak becomes narrower when u_{L} increases from 0 (black) to 0.5 (light blue) to 1.0 $k_{\mathrm{B}}T$ (blue). When u_{L} decreases from 0 (black) to -0.5 $k_{\mathrm{B}}T$ (light red), the single peak becomes wider, indicating a further local clustering of raft patches. At $u_{\mathrm{L}} = -1.0\,k_{\mathrm{B}}T$ (red), there appears a second peak corresponding to large raft domains. These distribution plots are consistent with the visual inspection of the snapshots. The evolution of different energies given by eqs. (1)-(5) in the adhesion systems with ligand-ligand interaction $u_{\mathrm{L}} = \pm1.0\,k_{\mathrm{B}}T$ is displayed in Figure a2 in Appendix.

The apparent equilibrium constant K for the receptor-ligand binding that causes the adhesion is also plotted in Figure 2(f) and found to decrease with u_{L}. This is related to

the physical fact that a receptor-ligand complex constrains the local separation between the two adhering surfaces and then suppresses the shape fluctuations of the cell membrane. The membrane conformational entropy thus induces an effective attraction between the complexes, see the cartoon in Figure 3(a). The attraction between ligands on the supported bilayers can cooperate with the membrane-mediated effective attraction and promote the formation of more complexes as well as receptor-containing raft domains, see Figure 3(b). On the contrary, the repulsion between ligand acts against the effective attraction between the complexes and therefore disfavors the receptor-ligand binding, see Figure 3(c). Our results suggest that the adhesion system is sensitive to the short-range interaction between the adjacent ligands on the supported bilayer.

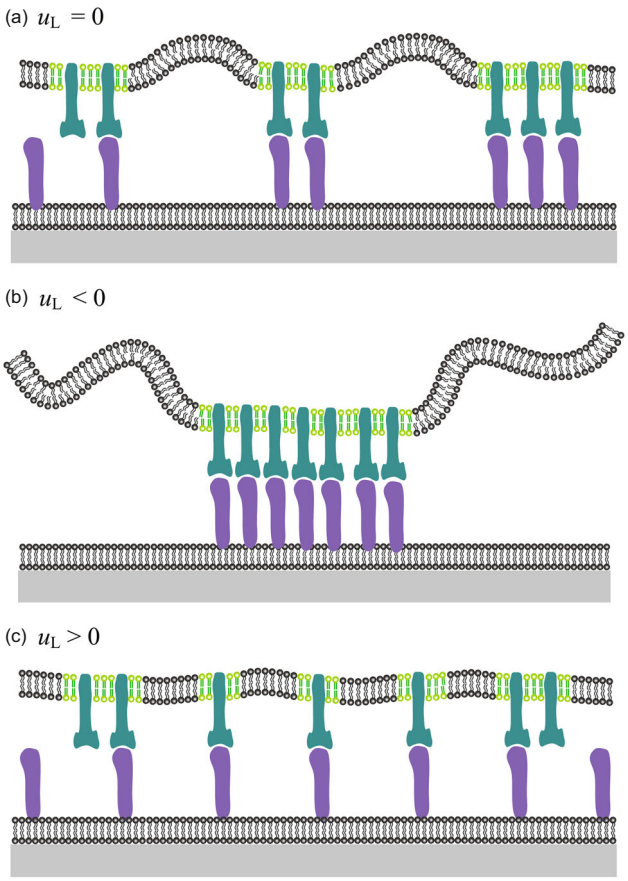

Figure 3 (Color online) Cartoons of the preferred configurations of the adhesion systems in different cases of ligand-ligand short-range interactions on the supported bilayer. (a) The membrane-mediated effective attraction between the receptor-ligand complexes enhances the coalescence of receptor-containing rafts, but might be insufficient to merge the multiple raft domains into one in the absence of ligand-ligand attraction ($u_L = 0$). (b) The strong ligand-ligand attraction, say $u_L = -1\,k_BT$, together with the membrane conformational entropy can overcome the translational entropy of ligands and receptor-containing rafts, leading to the formation of one mesoscale raft domain and large roughness of the cell membrane. (c) The strong ligand-ligand repulsion, e.g., $u_L \gtrsim 1\,k_BT$, acts against the membrane-mediated complex-complex attraction and disperses the complexes, which flattens the cell membrane.

To further explore the phase behavior, both MC simulations and MF calculations were performed for the adhesion systems that differ in ligand concentration c_L and ligand-ligand attraction u_L. The other parameters in these systems are $c_R = 1000\,\mu m^{-2}$, $x = 0.2$, $u_b = 6\,k_BT$, and $u_a = 3\,k_BT$. Control adhesion systems in which the adhering cell membranes are planar without shape fluctuations were also considered in order to appreciate the effective attraction between receptor-ligand complexes arising from the membrane conformational entropy. The resultant phase diagrams are shown in Figure 4 for different values of u_L. The points are identified from the peaks in the plots of heat capacity against raft-raft contact energy u in MC simulations (see Figure a1 in Appendix). The lines are from MF calculations as explained in sect. 2. For the sake of comparison, the critical value $u^* = -2\ln\left(1+\sqrt{2}\right)k_BT$ is used to rescale the MC data and $u^* = -k_BT$ the MF results. The lines exhibit systematic deviations from the points, but successfully capture the trends for the transition from the homogeneous to phase-separated state occurs with increasing c_L. In the phase-separated state, both the receptor-containing rafts and ligands form mesoscopic

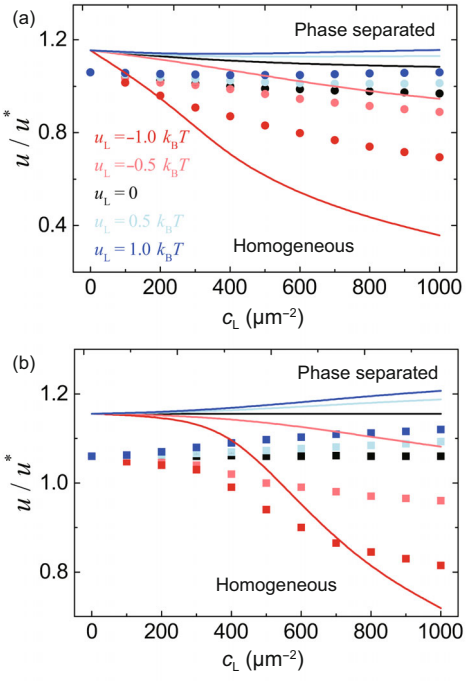

Figure 4 (Color online) Phase diagrams for the adhesion systems with (a) fluctuating or (b) planar cell membranes. The points are identified from the peaks in the plots of heat capacity C_V against u in MC simulations, whereas the lines are from MF calculations. For comparison, $u^* = -2\ln\left(1+\sqrt{2}\right)k_BT$ is used to rescale the MC data and $u^* = -1\,k_BT$ the MF results. The other parameters in the adhesion systems are the same as for Figure 2.

domains as illustrated in Figure 2(a). In the homogeneous state, the receptors, ligands and rafts are dispersed over the surfaces like gas, possibly forming small clusters, see Figure 2(b)-(e) for example. Figure 4(a) shows that, for c_L in the range of 100-1000 μm^{-2}, the presence of ligand-ligand repulsion ($u_L = 0.5$ and $1.0\,k_BT$) increases by at most 9% the raft-raft contact energy u for the phase separation to occur (blue, light blue versus black points), and the presence of ligand-ligand attraction ($u_L = -0.5$ and $-1.0\,k_BT$), however, decreases the value of u/u^* at the transition point by up to 29% (red, light red versus black points). In the control systems with planar cell membranes, the aforementioned membrane-mediated effective attraction between complexes does not exist, as evidenced by the unchanging value of u/u^* at the transition points when varying c_L in the absence of ligand-ligand interaction (black points in Figure 4(b)). Therefore, the transition points for the same set of c_L and u_L in Figure 4(b) are located at higher values of u/u^* than in Figure 4(a) as expected. The quantitative discrepancies between the MC and MF results arise from the fact that the MF approximation assumes the fluctuations of local composition variables n_i^+ and m_i^- around their average values are small.

Now we take a closer look at the receptor-ligand binding by analyzing the data from MC simulations. Figure 5(a) shows that the apparent binding constant $K = [RL]/([R][L])$ increases with the concentration c_L of ligands, regardless of the values of the ligand-ligand interaction strength u_L (circles). In the control systems with planar cell membranes (squares), K increases with c_L for $u_L < 0$ and decreases with c_L for $u_L > 0$. At $u_L = 0$, K remains constant and slightly exceeds $a^2 e^{u_b/k_BT}$, the binding constant in the dilute limit of receptors and ligands. The control systems exhibit larger values of K simply because the membrane conformational entropy disfavors the complex formation that restricts the local separation of the adhering surfaces in the systems with fluctuating cell membranes.

The role of ligand-ligand interaction and its interplay with the membrane-mediated attraction between the receptor-ligand complexes can be better visualized in the plots of log([RL]) versus log([R][L]) as shown in Figure 5(b). The lines are least square fits to the data points in the same color. The slope n of each line is then reflected in the law of mass action $[RL] \propto [R]^n[L]^n$ for the receptor-ligand binding. In the control systems, the relation $[RL] \propto [R][L]$ for non-cooperative binding is recovered in the absence of ligand-ligand interaction, i.e., $u_L = 0$ (black squares). An attraction of $u_L = -1.0\,k_BT$ induces the binding cooperativity (red squares, $n = 1.15 \pm 0.03$). A repulsion of $u_L = 1.0\,k_BT$ leads to weak anti-cooperativity of the binding (blue squares, $n = 0.95 \pm 0.01$). In contrast, the receptor-ligand binding in the adhesion systems with fluctuating cell membranes is cooperative with n dependent on u_L. At $u_L = 0$ (black circles), the law of mass action is very close to $[RL] \propto [R]^2[L]^2$ for the cooperative binding of adhesion receptors and ligands anchored to fluctuating and homogeneous membranes [20, 42]. Ligand-ligand attraction cooperates with the membrane-mediated attraction between the complexes and leads to $n > 2$ (red circles, $n = 4.12 \pm 0.3$), whereas ligand-ligand repulsion acts against the effective attraction and therefore weakens the binding cooperativity (blue circles, $n = 1.87 \pm 0.03$).

Since the MF theory gives the qualitatively correct phase diagrams as previously discussed, we constructed phase diagrams from MF calculations for the adhesion systems with different values of u_a and u_b. Figure 6(a) shows that, in the presence of ligand-ligand attraction ($u_L = -1.0\,k_BT$), the phase behavior of the adhesion systems is rather sensitive to the change in u_a and u_b. At a given concentration of ligands c_L, the phase separation occurs at lower values of u/u^* when increasing u_a (light red, red and black lines) or u_b (light blue, blue and red lines), because an increase in u_a or u_b leads to the formation of more receptor-ligand complexes that facilitates the coalescence of raft domains. Figure 6(b) shows that,

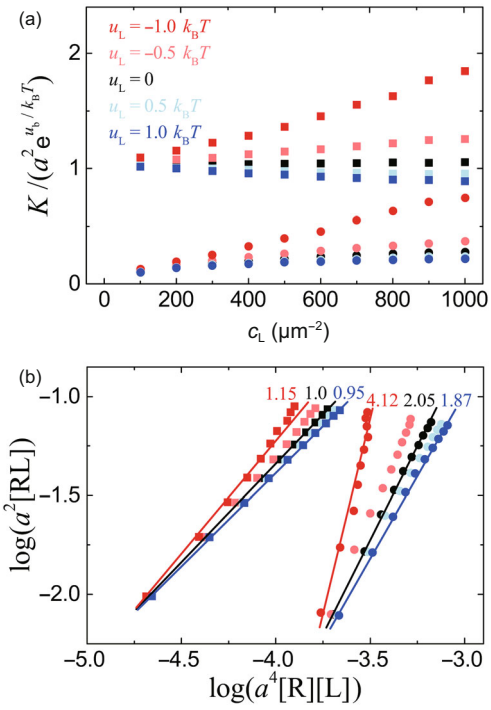

Figure 5 (Color online) Results for the receptor-ligand binding from MC simulations of the adhesion systems at different values of u_L for the ligand-ligand interaction. The choices for the other parameters in the adhesion systems are the same as for Figure 2. (a) Rescaled receptor-ligand binding constant $K/(a^2 e^{u_b/k_BT})$ versus ligand concentration c_L. (b) $\log(a^2[RL])$ versus $\log(a^4[R][L])$. The lines are least square fits to the data points with the slopes indicated by the numerical values. The data points in squares are from the control adhesion systems with planar cell membranes.

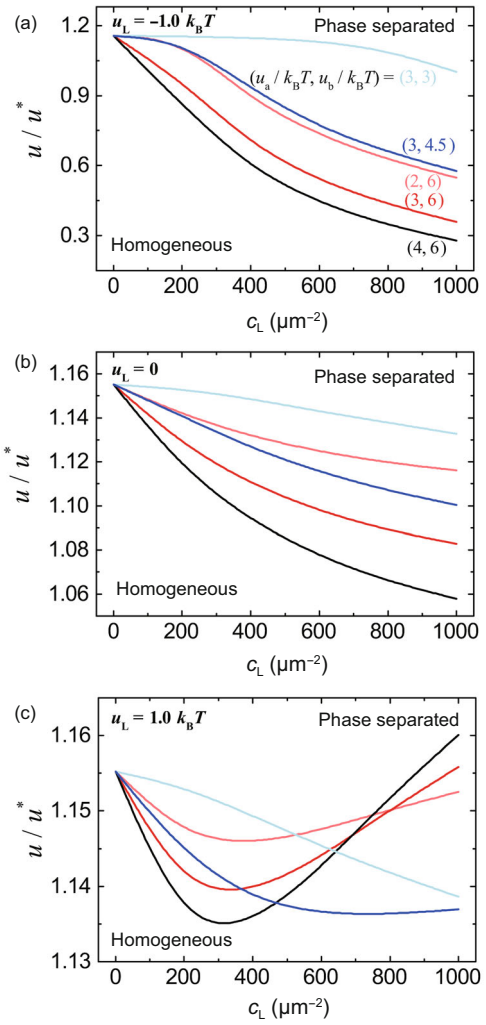

Figure 6 (Color online) Phase diagrams from MF calculations of the adhesion systems with different raft-receptor affinity u_a and receptor-ligand binding strength u_b for short-range ligand-ligand interaction (a) $u_L = -1.0\,k_BT$, (b) $u_L = 0$, and (c) $u_L = 1.0\,k_BT$. $u^* = -1k_BT$. The choices for the other parameters in the adhesion systems are raft area fraction $x = 0.2$ and area concentration of receptor $c_R = 1000\ \mu m^{-2}$.

in the presence of ligand-ligand repulsion ($u_L = 1.0\,k_BT$), the values of u/u^* at the phase boundaries change within 3% as u_a and u_b vary. For relatively weak binding ($u_b = 3\,k_BT$, light blue line), the value of u/u^* for phase separation to occur decreases monotonically with c_L, suggesting that the short-range ligand-ligand repulsion does not play a role when the average spacing between the complexes $\bar{d}_c = [RL]^{-1/2}$ is rather large. For strong binding ($u_b = 6\,k_BT$, light red, red and black lines), the phase boundaries are all concave with the lowest points slightly shifted to smaller values of c_L as increasing u_a, reflecting that the short-range ligand-ligand repulsion comes into effect when more complexes are formed.

Figure 7 shows the results for the receptor-ligand binding obtained from MC simulations of the adhesion systems with ligand-ligand attraction ($u_L = -1.0\,k_BT$) or repulsion ($u_L = 1.0\,k_BT$). Each data set in the same color is from the simulations with the specified values of u_a and u_b. An increase in the binding strength u_b leads to the formation of more receptor-ligand complexes (data points in light blue, blue, and red), irrespective of whether u_L is positive or negative. An increase in u_a does not necessarily lead to the formation of more complexes. In Figure 7(a), the binding constant K increases with u_a (data points in light red, red and black). In Figure 7(b), however, K decreases with u_a. This is because the binding of ligands to receptors preferentially localized in the raft domains gets more unfavorable by the ligand-ligand repulsion ($u_L = 1.0\,k_BT$) as u_a increases. In both Figure 7(a) and (b), the apparent binding constant K increases with the concentration of ligands c_L, indicating the cooperativity of the receptor-ligand binding that mediates the adhesion. Figure 7(c) and (d) show the corresponding plots of log([RL]) versus log([R][L]). As previously explained, the slope of each fitted line in such plots quantifies the binding cooperativity. The slope is found to increase considerably with increasing u_a and u_b at $u_L = -1.0\,k_BT$, and to decrease slightly with increasing u_a and u_b at $u_L = 1.0\,k_BT$ (light red, red and black lines; light blue, blue and red lines). Our results here demonstrate that the binding is more sensitive to the change in the ligand concentration in the case of ligand-ligand attraction than in the case of ligand-ligand repulsion.

4 Conclusions

We have investigated cell-SLB adhesion mediated by the binding of cell adhesion receptors to the SLB-tethered ligands that may experience short-range *cis*-interactions by using MC simulations and MF calculations based on a statistical-mechanical model. In the biologically relevant range of model parameters, our results show that the *cis*-interactions between adjacent ligands on the SLB can regulate the receptor-ligand binding and therefore the phase behavior of the adhesion system. More specifically, for the adhesion system with attractive ligand-ligand *cis*-interactions, we find that both the affinity and cooperativity of the receptor-ligand binding are enhanced. This enhancement can be attributed to the entropy gain of the cell membranes resulting from the attraction-induced protein aggregation. Contrary to the case of the homogeneous membrane without ligand-ligand *cis*-attraction where the receptor-ligand binding is weakened by the thermal shape fluctuations of the membranes, the membrane fluctuations actually function as a positive regulator for the binding in collaboration with the *cis*-attractive interactions of adjacent ligands. Meanwhile, the lipid rafts can be further stabilized and made to coalesce into mesoscale domains, thus facilitating the phase separa-

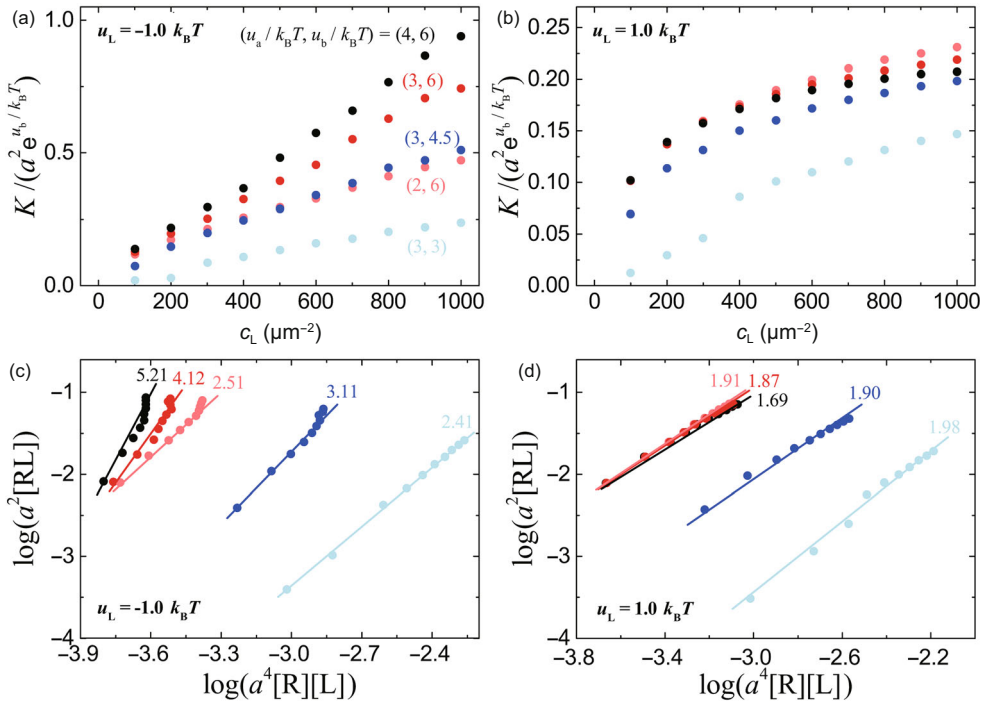

Figure 7 (Color online) Results for the receptor-ligand binding from MC simulations of the adhesion systems with different raft-receptor affinity u_a and receptor-ligand binding strength u_b at short-range ligand-ligand attraction $u_L = -1.0\,k_BT$ (a), (c) or repulsion $u_L = 1.0\,k_BT$ (b), (d). The other parameters are the same as for Figure 2. (a), (b) Rescaled receptor-ligand binding constant $K/(a^2e^{u_b/k_BT})$ versus ligand concentration c_L. (c), (d) $\log(a^2[RL])$ versus $\log(a^4[R][L])$. The lines are least square fits to the data points with the slopes indicated by the numerical values.

tion of the adhesion system, due to the presence of attractive ligand-ligand *cis*-interactions. Conversely, the repulsive ligand-ligand *cis*-interactions negatively affect the receptor-ligand binding and coalescence of lipid rafts by suppressing the protein aggregation and thermal shape fluctuations of cell membrane.

The adhesion of cell membranes to ligand-coated surfaces has been investigated with emphasis on the effects of thermally-excited membrane fluctuations [21], ligand mobility [37], external force [43,44], and surface morphology [45]. Our study here highlights the important role of ligand-ligand *cis*-interaction, which should be carefully taken into account in the cell-SLB adhesion experiments.

This work was supported by the National Natural Science Foundation of China (Grant Nos. 11902327, 21973040, and 11972041), Youth Innovation Promotion Association of Chinese Academy of Sciences, Strategic Priority Research Program of the Chinese Academy of Sciences (Grant No. XDB22040102), Fundamental Research Funds for the Central Universities (Grant No. 14380228), and Shenzhen Science and Technology Innovation Committee (Grant Nos. JCYJ20200109150656717, and JCYJ20170818110613113).

1 B. Alberts, A. Johnson, J. Lewis, D. Morgan, M. Raff, K. Roberts, and P. Walter, *Molecular Biology of the Cell* (Garland Science, New York, 2014).
2 Z. P. Xu, and Q. S. Zheng, Sci. China-Phys. Mech. Astron. **61**, 074601 (2018).
3 J. Li, D. Han, and Y. P. Zhao, Sci. Rep. **4**, 3910 (2014).
4 J. J. Li, and Y. P. Zhao, Chin. J. Theor. App. Mech. **44**, 807 (2012).
5 J. T. Groves, and M. L. Dustin, J. Immunol. Methods **278**, 19 (2003).
6 M. Tanaka, and E. Sackmann, Nature **437**, 656 (2005).
7 E. Sackmann, and A. S. Smith, Soft. Matter. **10**, 1644 (2014).
8 M. L. Dustin, M. E. Sanders, S. Shaw, and T. A. Springer, J. Exp. Med. **165**, 677 (1987).
9 K. H. Biswas, K. L. Hartman, C.-H. Yu, O. J. Harrison, H. Song, A. W. Smith, W. Y. C. Huang, W.-C. Lin, Z. H. Guo, A. Padmanabhan, S. M. Troyanovsky, M. L. Dustin, L. Shapiro, B. Honig, R. Z.-Bar, and J. T. Groves, Proc. Natl. Acad. Sci. USA **113**, E7870 (2016).
10 E. M. Schmid, M. H. Bakalar, K. Choudhuri, J. Weichsel, H. S. Ann, P. L. Geissler, M. L. Dustin, and D. A. Fletcher, Nat. Phys. **12**, 704 (2016).
11 G. Bell, Science **200**, 618 (1978).
12 M. L. Dustin, S. K. Bromley, M. M. Davis, and C. Zhu, Annu. Rev. Cell Dev. Biol. **17**, 133 (2001).
13 Y. Wu, J. Vendome, L. Shapiro, A. Ben-Shaul, and B. Honig, Nature **475**, 510 (2011).
14 T. R. Weikl, J. Hu, G. K. Xu, and R. Lipowsky, Cell Adhes. Migrat. **10**, 576 (2016).
15 J. Huang, V. I. Zarnitsyna, B. Liu, L. J. Edwards, N. Jiang, B. D. Evavold, and C. Zhu, Nature **464**, 932 (2010).
16 C. Zhu, W. Chen, J. Lou, W. Rittase, and K. Li, Nat. Immunol. **20**, 1269 (2019).
17 L. Limozin, P. Bongrand, and P. Robert, Sci. Rep. **6**, 35193 (2016).
18 D. T. L. Le, Y. Guérardel, P. Loubiére, M. Mercier-Bonin, and E. Dague, Biophys. J. **101**, 2843 (2011).
19 G. P. O'Donoghue, R. M. Pielak, A. A. Smoligovets, J. J. Lin, and J. T. Groves, eLife **2**, e00778 (2013).
20 H. Krobath, B. Różycki, R. Lipowsky, and T. R. Weikl, Soft. Matter. **5**, 3354 (2009), arXiv: 0906.0462.
21 J. Hu, R. Lipowsky, and T. R. Weikl, Proc. Natl. Acad. Sci. USA **110**, 15283 (2013).

22 G. K. Xu, J. Hu, R. Lipowsky, and T. R. Weikl, J. Chem. Phys. **143**, 243136 (2015).
23 J. Hu, G. K. Xu, R. Lipowsky, and T. R. Weikl, J. Chem. Phys. **143**, 243137 (2015), arXiv: 1511.07657.
24 L. Li, J. Hu, X. Shi, Y. Shao, and F. Song, Soft. Matter. **13**, 4294 (2017).
25 L. Li, J. Hu, B. Różycki, and F. Song, Nano Lett. **20**, 722 (2020).
26 J. Steinkühler, B. Różycki, C. Alvey, R. Lipowsky, T. R. Weikl, R. Dimova, and D. E. Discher, J. Cell Sci. **132**, jcs216770 (2019).
27 H. A. Anderson, E. M. Hiltbold, and P. A. Roche, Nat. Immunol. **1**, 156 (2000).
28 T. Murai, C. Sato, M. Sato, H. Nishiyama, M. Suga, K. Mio, and H. Kawashima, J. Cell Sci. **100**, (2013).
29 H. A. Anderson, and P. A. Roche, Biochim. Biophys. Acta (BBA) - Mol. Cell Res. **1853**, 775 (2015).
30 L. Li, X. Wang, Y. Shao, W. Li, and F. Song, Sci. China-Phys. Mech. Astron. **61**, 128711 (2018).
31 A. H. Bahrami, and T. R. Weikl, Nano Lett. **18**, 1259 (2018).
32 M. Knezevic, H. D. Jiang, and S. S. Wang, Nano Lett. **121**, 238101 (2018).
33 L. Li, J. Hu, G. Xu, and F. Song, Phys. Rev. E **97**, 012405 (2018).
34 P. K. Tsourkas, M. L. Longo, and S. Raychaudhuri, Biophys. J. **95**, 1118 (2008).
35 L. Li, J. Hu, L. Li, and F. Song, Soft. Matter. **15**, 3507 (2019).
36 B. Różycki, R. Lipowsky, and T. R. Weikl, New J. Phys. **12**, 095003 (2010), arXiv: 1007.3809.
37 L. Li, G. K. Xu, and F. Song, Phys. Rev. E **95**, 012403 (2017).
38 Y. Gambin, R. Lopez-Esparza, M. Reffay, E. Sierecki, N. S. Gov, M. Genest, R. S. Hodges, and W. Urbach, Proc. Natl. Acad. Sci. USA **103**, 2098 (2006).
39 S. Ramadurai, A. Holt, V. Krasnikov, G. van den Bogaart, J. A. Killian, and B. Poolman, J. Am. Chem. Soc. **131**, 12650 (2009).
40 K. Simons, and D. Toomre, Nat. Rev. Mol. Cell Biol. **1**, 31 (2000).
41 M. Fallahi-Sichani, and J. J. Linderman, PLoS ONE **4**, e6604 (2009).
42 L. Li, J. Hu, X. Shi, B. Różycki, and F. Song, Soft. Matter. **17**, 1912 (2021).
43 J. Qian, J. Wang, Y. Lin, and H. Gao, Biophys. J. **97**, 2438 (2009).
44 J. Qian, J. Lin, G. K. Xu, Y. Lin, and H. Gao, J. Mech. Phys. Solids **101**, 197 (2017).
45 S. Yu, H. Wang, Y. Ni, L. He, M. Huang, Y. Lin, J. Qian, and H. Jiang, Soft. Matter. **13**, 5970 (2017).

Appendix

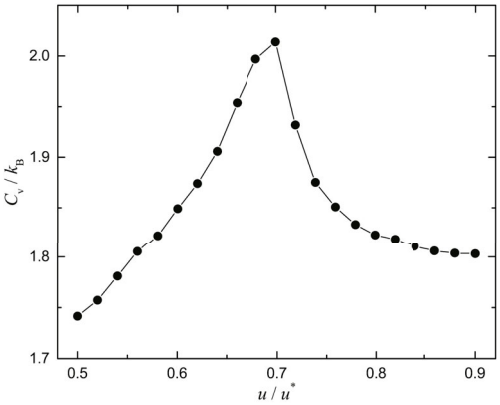

Figure a1 Heat capacity C_V versus contact energy U as obtained from MC simulations with raft area fraction $x = 0.2$, area concentration of receptors and ligands $c_R = c_L = 1000\ \mu m^{-2}$, receptor-ligand binding strength $u_b = 6\,k_BT$, raft-receptor affinity $u_a = 3\,k_BT$.

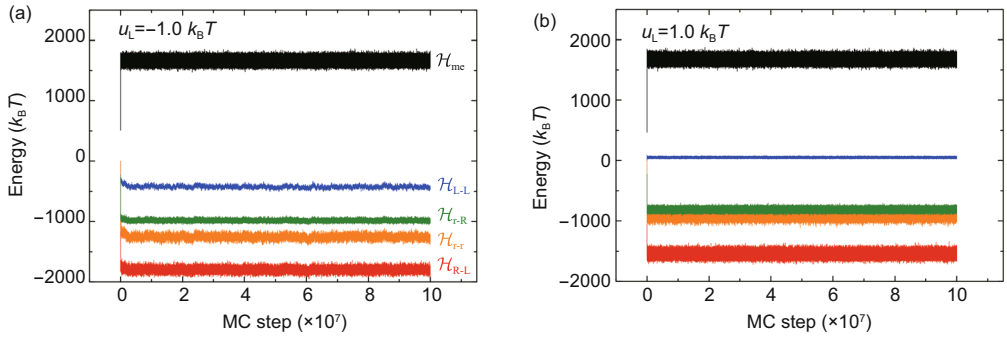

Figure a2 (Color online) The evolution of different energies in the adhesion system with ligand-ligand interaction (a) $u_L = -1.0\,k_BT$ and (b) $1.0\,k_BT$. The other parameters are the same as Figure 2.